

FLOW PHENOMENA IN ATLAS

A. ANDREAZZA, on behalf of the ATLAS Collaboration
INFN Sezione di Milano and Dipartimento di Fisica, Università di Milano
Via Celoria 16, I-20133, Milano, Italy

Measurements of flow anisotropy coefficients have been performed with the ATLAS detector at the LHC, on a sample of $8 \mu\text{b}^{-1}$ minimum bias Pb+Pb collisions at centre-of-mass energy $\sqrt{s_{\text{NN}}} = 2.76$ TeV and a sample of $1 \mu\text{b}^{-1}$ p +Pb collisions at $\sqrt{s_{\text{NN}}} = 5.02$ TeV. The large statistics Pb+Pb sample is used to derive event-by-event distribution of v_2 , v_3 and v_4 . Within uncertainties, the distributions of v_3 and v_4 agree with a pure Gaussian function over a wide centrality range, while significant deviations from this function are observed for v_2 in mid-central and peripheral collisions. In the p +Pb sample, a long-range near-side and away-side correlation is observed for events with high transverse energy in the detector. This structure can be described by v_2 anisotropy coefficients of magnitude similar to what is observed in Pb+Pb collisions.

1 Introduction

Heavy ion collisions at the Relativistic Heavy Ion Collider (RHIC) and the Large Hadron Collider (LHC) create hot, dense matter that is thought to be composed of strongly interacting quarks and gluons. A useful tool to study the properties of this matter is the azimuthal anisotropy of particle emission in the transverse plane.¹ This anisotropy is believed to result from pressure-driven anisotropic expansion (referred to as “flow”) of the created matter, and is described by a Fourier expansion of the particle distribution in azimuthal angle, around the beam direction:

$$\frac{dN}{d\phi} \propto 1 + 2 \sum_{n=1}^{\infty} v_n \cos n(\phi - \Phi_n) \stackrel{\text{def.}}{=} 1 + 2 \sum_{n=1}^{\infty} v_{n,x} \cos n\phi + v_{n,y} \sin n\phi, \quad (1)$$

where v_n and Φ_n represent the magnitude and phase of the n^{th} -order harmonics, respectively.

In this paper some recent measurements of the v_n in Pb+Pb and p +Pb collisions are presented.^{2,3,4} They are performed by the ATLAS detector⁵ at the LHC, using the charged particles reconstructed in the inner detector, within its acceptance in pseudorapidity $|\eta| < 2.5^a$. The event centrality is derived from the transverse energy deposition in the forward calorimeter (FCal) covering $3.2 < |\eta| < 4.9$.⁶

The data samples were collected with a minimum bias trigger. They consist of $8 \mu\text{b}^{-1}$ integrated luminosity of Pb+Pb collisions at $\sqrt{s_{\text{NN}}} = 2.76$ TeV from the 2010 LHC run, and of $1 \mu\text{b}^{-1}$ integrated luminosity of p +Pb collisions at $\sqrt{s_{\text{NN}}} = 5.02$ TeV from a short pilot run in September 2012.

^aATLAS uses a right-handed coordinate system with its origin at the nominal interaction point (IP) in the centre of the detector and the z -axis along the beam pipe. The x -axis points from the IP to the centre of the LHC ring, and the y -axis points upward. Cylindrical coordinates (r, ϕ) are used in the transverse plane, ϕ being the azimuthal angle around the beam pipe. The pseudorapidity is defined in terms of the polar angle θ as $\eta = -\ln \tan(\theta/2)$.

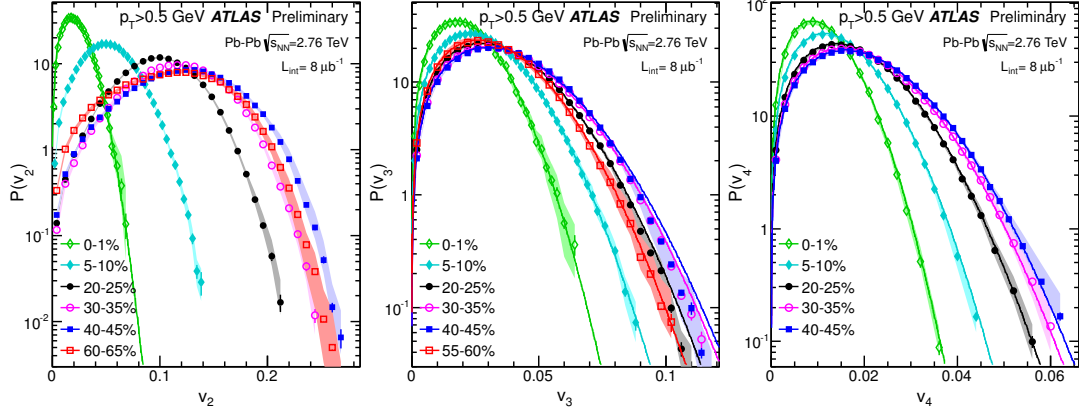


Figure 1: The probability distribution of the Ebe v_n in several centrality intervals for $n=2$ (left panel), $n=3$ (middle panel) and $n=4$ (right panel). The errors bars are statistical uncertainties, and the shaded bands are uncertainties on the v_n -shape. The solid curves are distributions calculated from the measured $\langle v_n \rangle$ according to Eq. 2; they are shown for the 0-1% centrality interval for v_2 , but for all centrality intervals for v_3 and v_4 .²

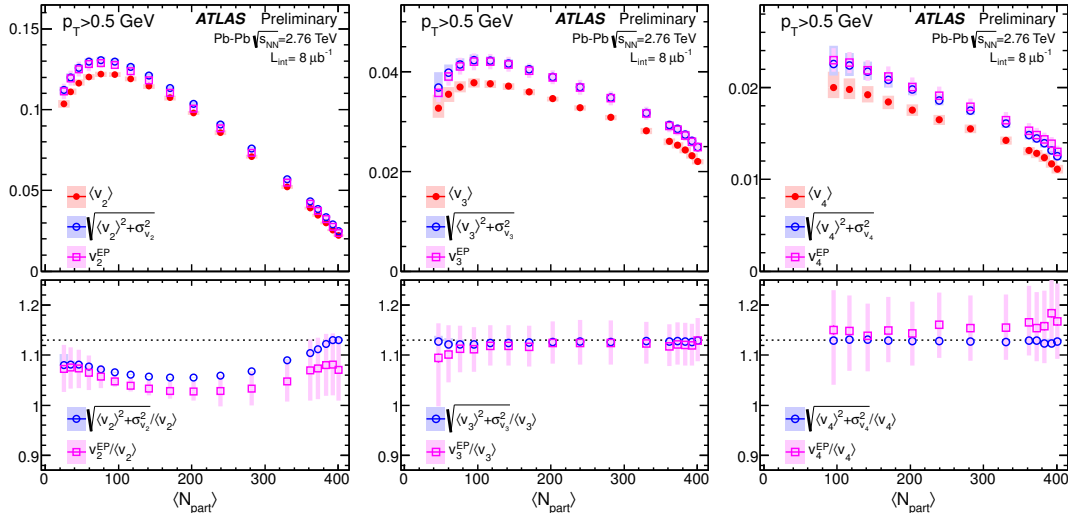


Figure 2: Top panels: Comparison of $\langle v_n \rangle$ and $\sqrt{\langle v_n^2 \rangle} = \sqrt{\langle v_n \rangle^2 + \sigma_n^2}$ derived from the Ebe v_n distributions with the v_n^{EP} , for charged particles with $p_T > 0.5$ GeV. Bottom panels: the ratios of $\sqrt{\langle v_n^2 \rangle}$ and v_n^{EP} to $\langle v_n \rangle$. The shaded bands represent the systematic uncertainties. The dotted lines in bottom panels indicate $\sqrt{\langle v_n^2 \rangle} / \langle v_n \rangle = 1.13$, expected for the radial projection of a 2D Gaussian distribution.²

2 Event-by-Event distributions

The average values of v_n and their dependence on centrality, p_T and η , have been measured at the LHC^{7,8,9} with different techniques. In particular the “elliptic flow”, v_2 , has large values reflecting the shape of the overlapping nuclei.^{10,11,12} The Fourier coefficients in Eq. 1 can also be computed on an event-by-event (Ebe) basis from the particle azimuthal distribution.²

The measured distributions for $v_n = \sqrt{v_{n,x}^2 + v_{n,y}^2}$ ($n = 2-4$), after unfolding for the smearing due to finite charged particle multiplicity, are shown in Figure 1. The remaining width is expected to reflect fluctuations in the initial state geometry. In case of pure Gaussian fluctuations, the distributions would be described by the radial projection of a 2D Gaussian distribution:

$$P(v_n) = \frac{v_n}{\delta_n^2} e^{-\frac{v_n^2}{2\delta_n^2}}, \quad \langle v_n \rangle = \sqrt{\frac{\pi}{2}} \delta_n, \quad \sigma_n^2 = \langle v_n^2 \rangle - \langle v_n \rangle^2 = \left(2 - \frac{\pi}{2}\right) \delta_n^2. \quad (2)$$

The data show this is the case for v_3 and v_4 on a wide centrality range, and for v_2 in the most central events. For less central events, v_2 has a significant contribution from the shape

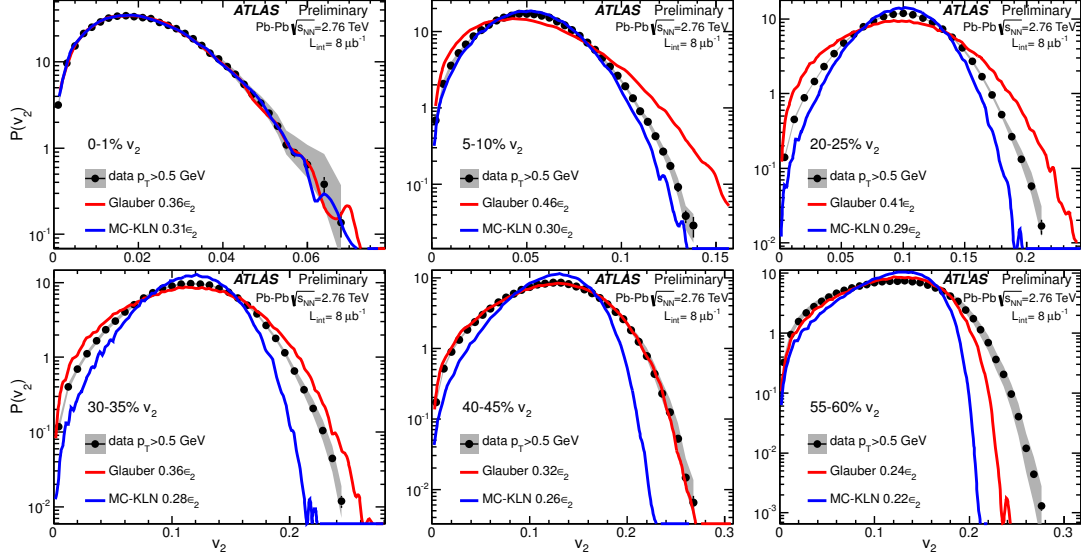


Figure 3: The EBe v_2 distributions compared with the eccentricity distributions from two initial geometry models: a Glauber model¹³ (red lines) and the MC-KLN model¹⁶ (blue lines).²

of the overlapping region between the interacting nuclei. This is quantitatively illustrated in Fig. 2 where the values of $\sqrt{\langle v_n^2 \rangle} / \langle v_n \rangle$ obtained by the v_n distributions are compared with the expectation from Eq. 2, as a function of the average number of participants in each centrality interval, $\langle N_{\text{part}} \rangle$, as estimated from a Glauber model Monte Carlo.¹³ In this Figure, $\sqrt{\langle v_n^2 \rangle}$ is also compared with the v_n^{EP} obtained by the event plane method.⁹ This method is expected to give $\langle v_n \rangle < v_n^{\text{EP}} < \sqrt{\langle v_n^2 \rangle}$, the actual value being experiment-dependent.¹⁴ The published ATLAS values of v_n^{EP} are very near to the upper bound.

If anisotropy is due to the hydrodynamic expansion of the strongly interacting system, the v_n is expected to scale with the eccentricity ε_n obtained by averaging the positions of the participating nucleons with respect to their centre-of-mass, in the transverse $r - \phi$ plane:¹⁵

$$\varepsilon_n = \frac{\sqrt{\langle r^n \cos n\phi \rangle^2 + \langle r^n \sin n\phi \rangle^2}}{\langle r^n \rangle}. \quad (3)$$

In Fig. 3 the eccentricity distribution ε_2 is computed using a Glauber model¹³ and the MC-KLN model¹⁶, and rescaled to the average v_2 distribution. The rescaled ε_2 of both models describe the data well in the 1% most central collisions, but start to fail towards less central events. Neither model describes the more peripheral data well.

3 The ridge in p +Pb collisions

Proton-nucleus collisions at the LHC are crucial for the interpretation of results from the Pb+Pb program.¹⁷ In particular, the relationship between fluctuations in the initial geometry and final-state particle correlations can be further investigated by studying correlations in p +Pb collisions with observables such as the two particle correlation function³ and the two- and four-particle cumulants.⁴ These observables are studied as a function of the transverse energy deposited on the FCal in the side of the outgoing Pb beam, $\sum E_T^{\text{Pb}}$, and of the particle p_T .

Figures 4a and 4b show two-particle correlation function, $C(\Delta\eta, \Delta\phi)$, at low and high $\sum E_T^{\text{Pb}}$, respectively. At high $\sum E_T^{\text{Pb}}$ a ‘‘ridge’’, a long-range correlation in $\Delta\eta$ at $\Delta\phi \sim 0$, is evident. The recoil component at $\Delta\phi \sim \pi$ is also enhanced. The amount of correlated pairs is evaluated using the per-trigger yield¹⁸ after subtracting the pedestal of uncorrelated pairs (zero-yield at minimum, ZYAM, method), as shown in Figure 4c. At low $\sum E_T^{\text{Pb}}$ only a recoil contribution is

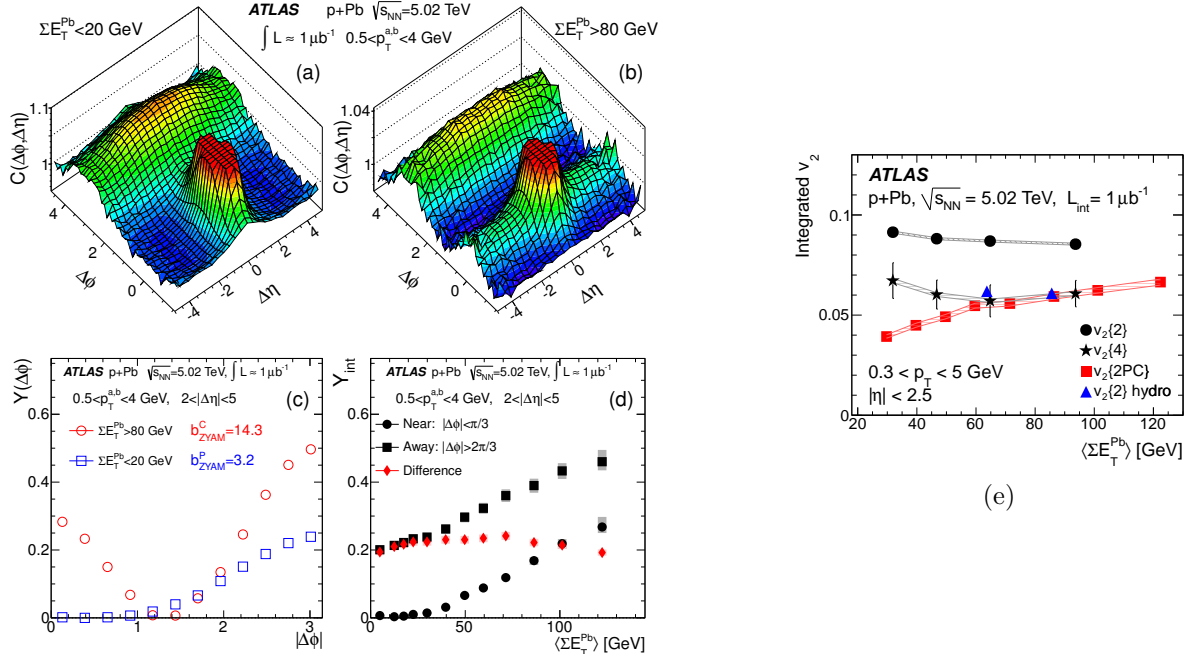


Figure 4: Two-dimensional correlation functions for (a) peripheral events and (b) central events, both with a truncated maximum to suppress the large correlation at $(\Delta\eta, \Delta\phi) = (0, 0)$; (c) the per-trigger yield $\Delta\phi$ distribution together with pedestal levels for peripheral (b_{ZYAM}^P) and central (b_{ZYAM}^C) events, and (d) integrated per-trigger yield as function of $\sum E_T^{Pb}$ for pairs in $2 < |\Delta\eta| < 5$. The shaded boxes represent the systematic uncertainties, and the statistical uncertainties are smaller than the symbols.³ (e) The second-order harmonic, v_2 , calculated with two- and four-particle cumulants (circles and stars, respectively), as a function of $\sum E_T^{Pb}$. Systematic uncertainties are shown as shaded bands. Also shown is $v_2\{2PC\}$ from two-particle correlations (squares) and predictions from a hydrodynamic model²² (triangles) for the same selection of charged particles as in the data.⁴

visible at $|\Delta\phi| \sim \pi$. At high $\sum E_T^{Pb}$ a correlated component appears at $|\Delta\phi| \sim 0, \pi$. Figure 4d displays the per-trigger yields integrated on the “near” ($|\Delta\phi| < \pi/3$) and the “away” ($|\Delta\phi| > 2\pi/3$) sides as a function of $\sum E_T^{Pb}$. Both regions show a correlated rise with transverse energy, with same magnitude in the near- and away-side.

In order to quantify this rise, the yield of low $\sum E_T^{Pb}$ events is subtracted from high $\sum E_T^{Pb}$ events. This difference as a function of $\Delta\phi$ can be described mostly by a $\cos(2\Delta\phi)$ modulation. Such a feature in the two-particle correlation function can be converted into a v_2 Fourier coefficient of the single-particle distribution of Eq. 1.⁹ These coefficients, $v_2\{2PC\}$, are compared in Figure 4e with $v_2\{2\}$ and $v_2\{4\}$ obtained by the two- and four-particle cumulants.¹⁹ The large magnitude of $v_2\{2\}$ compared to $v_2\{4\}$ suggests a substantial contamination from non-flow correlations. The four-particle cumulant shows a value of approximately 0.06, which agrees with $v_2\{2PC\}$ at high $\sum E_T^{Pb}$. The disagreement at low $\sum E_T^{Pb}$ could be due either to the subtraction procedure in the $v_2\{2PC\}$ determination or to residual non-flow effects in $v_2\{4\}$.

The p_T -dependence of v_2 has also been studied and the trend in $p+Pb$ collisions is similar to what observed in $Pb+Pb$ collision, with a magnitude between that measured in the most central and peripheral $Pb+Pb$ collisions.^{9,10} Comparable magnitude of v_2 has also been reported by ALICE²⁰ and can be possibly explained within the colour glass condensate and hydrodynamic models^{21,22}

4 Conclusions

The high statistics $Pb+Pb$ samples collected by the ATLAS experiment at the LHC allow for studies of flow phenomena with a wide range of analysis techniques.^{9,10,11,12,23} In particular the Fourier coefficients of the anisotropy flow can be measured on an event-by-event basis, accessing their fluctuations.² The resulting v_3 and v_4 distributions are compatible with Gaussian

fluctuations on a wide rapidity range, while for v_2 there is a significant contribution from the initial shape of the overlapping nuclei. The observed distributions cannot be described by basic Glauber models.

Already the initial pilot run of p +Pb collision at the LHC has provided interesting observations. In high transverse energy events, the ridge in the two particle correlation function shows a flow-like anisotropy, dominated by a term $v_2 \approx 0.06$,^{3,4} comparable to the value observed in Pb+Pb collisions.

References

1. J.-Y. Ollitrault, *Phys. Rev. D* **46**, 229 (1992).
2. ATLAS Collaboration, ATLAS-CONF-2012-114, [<http://cdsweb.cern.ch/record/1472935>].
3. ATLAS Collaboration, *Phys. Rev. Lett.* **110**, 182302 (2013), [arXiv:1212.5198].
4. ATLAS Collaboration, submitted to *Phys. Lett. B*, [arXiv:1303.2048].
5. ATLAS Collaboration, JINST **3**, S08003 (2008).
6. ATLAS Collaboration, *Phys. Lett. B* **710**, 363 (2012) [arXiv:1108.6027].
7. ALICE Collaboration, *Phys. Lett. B* **708**, 249 (2012), [arXiv:1109.2501].
8. CMS Collaboration, *Eur. Phys. J. C* **72**, 2012 (2012), [arXiv:1201.3158].
9. ATLAS Collaboration, *Phys. Rev. C* **86**, 014907 (2012), [arXiv:1203.3007].
10. ATLAS Collaboration, *Phys. Lett. B* **707**, 330 (2012), [arXiv:1108.6018].
11. ATLAS Collaboration, ATLAS-CONF-2012-117, [<http://cdsweb.cern.ch/record/1472939>].
12. ATLAS Collaboration, ATLAS-CONF-2012-118, [<http://cdsweb.cern.ch/record/1472940>].
13. M. L. Miller, K. Reygers, S. J. Sanders and P. Steinberg, *Ann. Rev. Nucl. Part. Sci.* **57**, 205 (2007).
14. M. Luzum and J.-Y. Ollitrault, *Phys. Rev. C* **87**, 044907 (2013), [arXiv:1209.2323].
15. G.-Y. Qin, H. Petersen, S. A. Bass, and B. Muller, *Phys. Rev. C* **82**, 064903 (2010), [arXiv:1009.1847].
16. A. Adil, H. J. Drescher, A. Dumitru, A. Hayashigaki and Y. Nara, *Phys. Rev. C* **74**, 044905 (2006), [arXiv:nucl-th/0605012]; H. J. Drescher and Y. Nara, *Phys. Rev. C* **75**, 034905 (2007) [arXiv:nucl-th/0611017].
17. C. Salgado *et al.*, *J. Phys. G* **39**, 015010 (2012), [arXiv:1105.3919].
18. CMS Collaboration, *Phys. Lett. B* **718**, 795 (2012), [arXiv:1210.5842].
19. N. Borghini, P. M. Dinh and J. -Y. Ollitrault, *Phys. Rev. C* **63**, 054906 (2001).
20. ALICE Collaboration, *Phys. Lett. B* **719**, 29 (2012), [arXiv:1212:2001].
21. K. Dusling and R. Venugopalan, *Phys. Rev. D* **87**, 054014 (2013), [arXiv:1211.3701].
22. P. Bożek and W. Broniowski, *Phys. Lett. B* **718**, 1557 (2013), [arXiv:1211.0845].
23. ATLAS Collaboration, ATLAS-CONF-2012-049, [<http://cdsweb.cern.ch/record/1451882>].